6. Developments on vegetable fibre-cement based materials in Sao Paulo, Brazil: an overview / V. Agopyan [et al.] // Cement and Concrete Composites. – 2005. – No. 27 (5). – P. 527–536.

7. Fiore, V. Characterization of a new natural fiber from Arundo donax L. as potential reinforcement of polymer composites / V. Fiore, T. Scalici, A. Valenza // Carbohydrate Polymers. – 2014. – No. 106. – P. 77–83.

8. Non-conventional cement-based composites reinforced with vegetable fibers / F. Santos [et al.] // A review of strategies to improve durability. Materiales de Construcciòn. – No. 65 (317). – 2015. – P. 1–20.

UDC 666.972:539.421.2

METODOLOGY OF STUDY OF THE STRUCTURE OF CEMENT MATERIALS BY THE METHOD OF NANOINDENTATION

E. N. Polonina[1], S. N. Leonovich[1,2], O. Lahayne[3], J. Eberhardsteiner[3], V. V. Potapov[4], S. A. Zhdanok[5]

[1] Belarusian National Technical University, Minsk, grushevskay_en@tut.by
[2] Qingdao University of Technology, China, Qingdao
[3] Vienna University of Technology, Austria, Vienna
[4] Research Geotechnological Center, Far Eastern Branch of the Russian Academy of Sciences, Russia, Petropavlovsk-Kamchatsky
[5] Advanced research and technology, Belarus, Minsk

Abstract

The parameters of the nanoindentation method were selected to ensure the final consistent results were obtained. These results are presented by histograms of the distribution of nanoindentation points by elasticity and hardness moduli and distributions by these characteristics in the horizontal XY plane perpendicular to the movement of the nanoindenter. It was revealed that the elastic modulus increases in samples that contain a complex additive containing nano-sized particles. The effect is also observed when introducing an additive containing only one type of nanoparticles (hydrothermal SiO_2 nanoparticles or multiwalled carbon nanotubes MWCNTs. Studies of cement stone samples at W/C = 0,21 and the content of SiO_2 in the combined additive is 0,000006 wt. % and MWCNT 0,00004 wt. % for cement showed that the effect of nanoparticles on the structure of the CSH gel becomes more pronounced, because the volume fraction of the LD phase of the CSH gel with a low packing density of nanograins becomes significantly lower than the fraction of the HD phase with an increased hexagonal packing density of granules. The results obtained indicate that there is a change in the nanostructure of the C–S–H gel, which is compared with an increase in strength, Young's and shear moduli with the introduction of SiO_2 nanoparticles and MWCNT nanoparticles. Using the nanoindentation method, it becomes possible to explain the nanogranular nature of the CSH gel, which is characteristic and determined by the contact forces of the CSH gel particles for these phases.

Keywords: nanoparticles, nanoindentation, nanogranules, packing density.

Introduction

In recent years, interest in the study of the properties and processes of obtaining and using nanomaterials, the range of use of which is steadily expanding, has increased significantly. The development of nanotechnology makes it possible to solve a number of problems in building materials science: increasing strength, durability, abrasion resistance, and corrosion resistance, which determines the operational reliability of building structures. This is mainly achieved by modifying the structure and properties of existing materials or products with nanoparticles introduced into their volume or onto the surface layer [1–16].

Hydration of cement materials is accompanied by the formation of calcium hydrosilicates (CSH). Accordingly, the hydration process is completed in the early, middle and late periods, resulting in the formation of two types of CSH phases: low density (LD) and high density (HD). Under normal conditions, LD CSH is usually formed in the middle stage, while HD CSH formation predominates in the later stage.

To reveal the relationship between the morphology and mechanical properties of CSH, a nanoindentation technique is used, which primarily reveals differences in structure. During nanoindentation, most solid non-metallic materials, such as concrete, are deformed elastically-plastically, which makes it possible to characterize mechanical properties such as hardness (H) and elastic modulus (E). Nanoparticles of different chemical compositions with a high specific surface area and high surface energy are used to specifically influence the nanostructure of the CSH gel. And the nanoindentation method makes it possible to evaluate the effect of nanoparticles directly on the volume fraction of different forms of CSH gel in early and adulthood.

Based on the results obtained using a number of methods, new ideas have emerged about the kinetics of formation and structure of the gel of calcium silicate hydrates – CSH (size, shape, density, etc.). CSH gel holds concrete in a solid, solid state and is itself a nanomaterial. At a small scale (1–5 nm), the CSH gel has a layer structure, and the layers tend to cluster into compact domains in which the distances between individual CSH layers are on the order of several nanometers. On a larger scale (from 5 to 100 nm), domains form three-dimensional disk-shaped structures with dimensions of 60 x 30 x 5 nm3 (5 nm thickness, long axis about 60 nm) – the so-called CSH particles [3–6]. During the hydration process, the number of CSH particles increases, the particles aggregate, forming three types of amorphous CSH gel at the microlevel (1 μm): 1) LD Low density CSH gel; 2) HD High density CSH gel; 3) UD CSH gel with ultra-high density. The three varieties of CSH gel exhibit different mechanical properties: high and ultra-high density CSH gel have higher stiffness and hardness compared to low density CSH gel. The volumetric proportion in concrete between varieties of CSH gel depends on the cement and mixing conditions, but the mechanical properties (modulus of elasticity, hardness) of high and low density CSH gel do not change when moving from one cement to another. [7]. The boundaries between the phases are quite arbitrary, but nevertheless they exist. High statistical deviations for the average values of E and H indicate that the samples within their volume are heterogeneous in their E and H characteristics.

Using nanoindentation, atomic force microscopy, and small-angle neutron scattering methods, the nanogranular structure of the CSH gel was established [2–3].

The consequence of the granular structure is the dependence of the volumetric elastic modulus K, shear modulus G, elastic modulus M and hardness H on the volumetric packing density η of CSH gel nanoparticles, which subsequently affects the macromechanical strengths in compression, bending, axial tension, etc., and the porous structure of the material. In normalized coordinates, these dependences are quite universal, and are weakly influenced by such factors as the water-cement ratio W/C, the degree of hydration and brand of Portland cement, the age of the sample, the aspect ratio of hydrosilicate-calcium particles, as well as the origin of calcium-silicate particles: a) technogenic hydrosilicates-calcium – products of hydration of Portland cement, b) calcium silicates of shales and other rocks, c) calcium silicates of the mineral component of the bones of animal organisms [2].

Work [3] provides equations relating E, H to the volumetric packing density. Mechanical properties (M, H) increase with packing density, as is the matching of nanoindentation modulus and hardness, as well as characteristic packing densities. In addition, to evaluate the relationship between the composite indentation modulus M and the elastic modulus of the solid m_s (Eq. 1) as a function of the ratio of the shear modulus of the composite material $G = g_s$, the volumetric shear modulus of the solid the ratio $r_s = k_s / g_s$ and packing density η [2, 3]

$$\frac{M}{m_s} = F_{sc}(\eta, r_s) = \frac{G}{g_s} \frac{(9\eta r_s + 4G/g_s + 3r_s)(3r_s + 4)}{4(4G/g_s + 3r_s)(3r_s + 1)} \quad . \tag{1}$$

In particular, the Poisson's ratio of a solid body $\nu_s = 1/5$ ($r_s = 4/3$) gives a linear scaling of all elastic properties with packing density (Eq. 2):

$$\frac{M}{m_s} = F_{sc}(\eta, r_s = 4/3) = 2\eta - 1 \quad . \tag{2}$$

A similar approach is used for normalized hardness:

$$\frac{H}{h_s} = \Pi_H = \Pi_1(\eta) + \mu(1-\eta)\Pi_2(\mu, \eta) \, . \tag{3}$$

Where

$$\Pi_1(\eta) = \frac{\sqrt{2(2\eta - 1)} - (2\eta - 1)}{\sqrt{2} - 1} (1 + a(1-\eta) + b(1-\eta)^2 + c(1-\eta)^3) \, . \tag{4}$$

$$\Pi_2(\mu, \eta) = \frac{2\eta - 1}{2} (d + e(1-\eta) + f(1-\eta)\mu + g\mu^3) \, , \tag{5}$$

and where a = – 5,3678, b = 12,1933, c = – 10,3071, d = 6,7374, e = – 39,5893, f = 34,3216 and g = – 21,2053 – all constants associated with the geometry of the Berkovich indenter and the morphology of the polycrystal with the percolation threshold $\eta_0 = 0{,}5$.

According to nanoindentation data of cement-water samples, the volume fraction of CSH gel phases with different packing densities of granules LD, HD, UHD largely depends on the W/C ratio ([2], Figure 1).

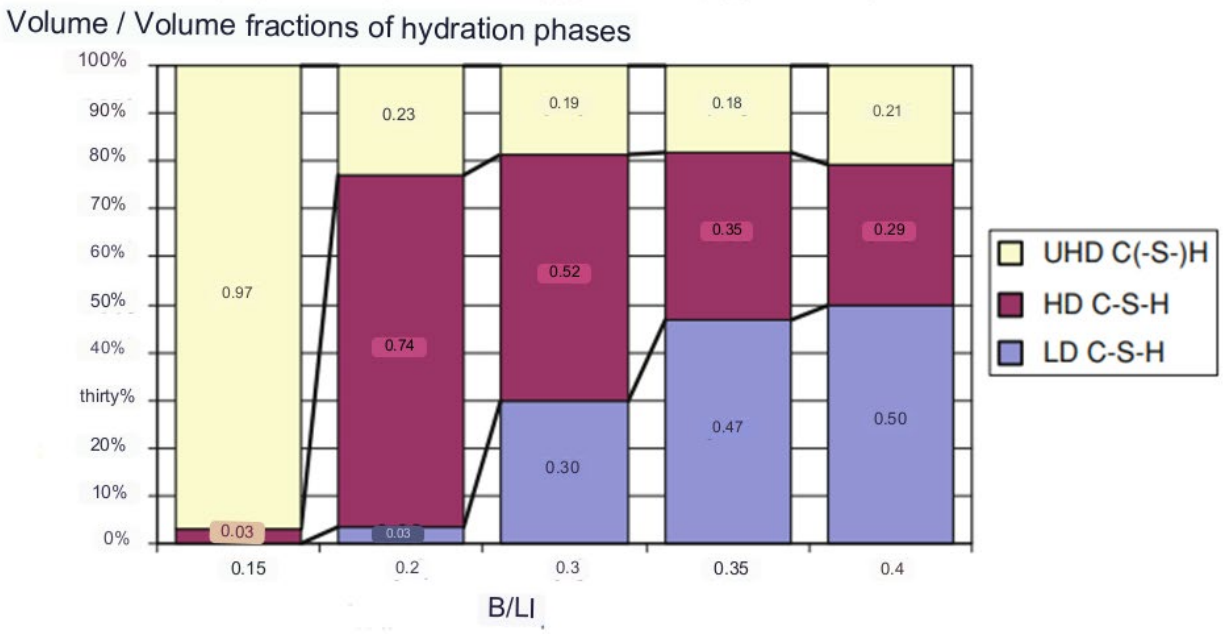

Figure 1 *– Distribution of volume fractions in the microstructure*

At the age of 6 months. at W/C = 0,2, the volume fraction of non-hydrated cement is 30 %, the fraction of hydration products is 54 %, and the fraction of gel porosity is 16 %. For W/C = 0,2, a very low proportion of the LD phase of the CSH gel is characteristic – 3 % in relation to phases with an increased particle packing density. According to equations (2) and (3), the result of the effect of nanoparticles on M, H and on the volume fractions of the gel phases at one W/C value can be recalculated to any other W/C value, using an additional bar diagram of the volume fractions of the phases (Figure 1).

According to atomic force microscopy and nanoindentation in layers of calcium hydrosilicates formed from a solution of sodium silicate on the surface of calcium carbonate in the presence of various amounts of Ca $(OH)_2$, CSH nanoparticles have dimensions of 5 x 30 x 60 nm ^{3} and are characterized by modulus M in the direction perpendicular to the surface about 200 GPa and in the longitudinal – about 50 GPa [10]. In this case, the mechanical characteristics of continuous CSH nanoparticles decrease with a decrease in the concentration of Ca $(OH)_2$ during the preparation of CSH particles.

The introduction of nanoparticles into the water-cement system allows you to specifically increase the volume fraction of the HD phase CSH gel with hexagonal packing of particles (η = 0,76) and reduce the volume fraction of the LD phase CSH gel with cubic packing (η = 0,64), accordingly, increase the elastic modulus and hardness of the CSH gel, which are directly proportional to the volumetric packing density of the particles.

The purpose of this work was to use nanoindentation to determine the effect of hydrothermal SiO_2 nanoparticles and MWCNT nanoparticles included in the combined additive directly on the volume fraction of different forms of CSH gel, thereby confirming the nanogranular nature of the CSH gel.

Experimental program

Nanoindentation technique and materials. Method used nanoindentation, when a solid needle of a known shape is pressed into the surface of a cement stone sample at a constant speed. When the specified load or indentation depth is reached, the movement stops for a certain time, after which the needle is retracted in the opposite direction. During the loading process, the load values and the corresponding indenter displacement are recorded. The resulting relationship is called the loading/unloading curve (Figure 2).

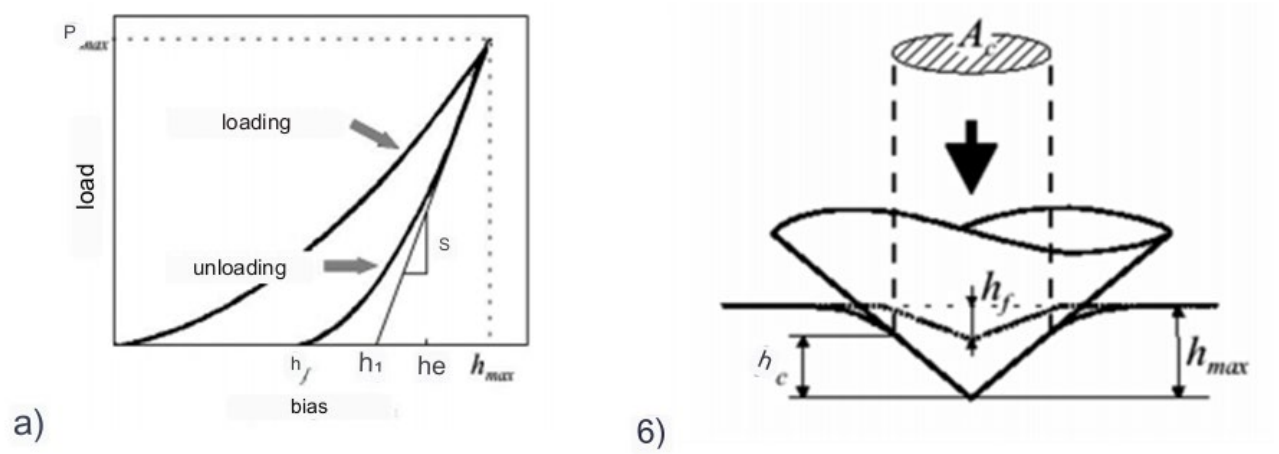

a) loading curve *P* (*h*); b) measurement scheme

Figure 2 *– Algorithm for measuring hardness using the nanoindentation method*

From this experimental curve, the hardness and elastic modulus of the material can be determined. Within the method proposed by Oliver and Far, the hardness *H* of a sample is given by the equation

$$H = \frac{P_{\max}}{A_c}, \tag{6}$$

where A_c is the projection area of the print at the maximum value of the applied load $P_{\max}$ (Fig. 2, *b*). Effective elastic modulus value

$$E_r = \frac{1}{\beta}\frac{\sqrt{\pi}}{2}\frac{S}{\sqrt{A_c}}. \tag{7}$$

A_c is the contact area of the Berkovich diamond tip with the sample at a given immersion depth h_c.

The constant βdepends on the shape of the indenter. For a Berkovich indenter with an apex angle of 142º β = 1,034.

The contact stiffness *S* is determined by the slope of the initial part of the unloading curve *Pmax*_

$$S = \left(\frac{dP}{dh}\right)_{P=P_{\max}}. \tag{8}$$

The greatest depth of penetration of the indenter into the surface h_c is calculated by the formula

$$h_c = h_{\max} - \varepsilon\frac{P_{\max}}{S} = h_{\max} - \varepsilon\left(h_{\max} - h_i\right). \tag{9}$$

The constant ε depends on the geometry of the indenter (ε~0,75 for the Berkovich pyramid), h_i – the distance corresponding to the intersection of the tangent to the unloading curve in the initial part with the axis of penetration (Figure 2*a*).

The projection area A_c is determined from a predetermined function of the indenter shape $A(h)$ when substituting the calculated value of the contact depth hc

$$A_c = A(h_c). \tag{10}$$

The tip shape function represents the dependence of the cross-sectional area of the tip A on the distance along the indenter axis h. Within the framework of this method, the function $A(h)$ n is assumed to be known in advance. In this work, research was carried out using an automated nanoindenter Hysitron TI 950 TriboIndenter. When performing mechanical measurements, a diamond probe tip was used.

M was 1.5 GPa (m = 100 intervals within 0–150 – GPa), the step in H was 0,1 GPa (100 intervals within 0–10 – GPa). The experimental results are presented as histograms of the distribution of nanoindentation points according to the reduced elastic modulus M and hardness H. Deconvolution over three phases J = 1, 2, 3 values $x = M$, H was performed according to the normal Gaussian distribution for each J phase

$$p_j(x) = \frac{1}{\sqrt{2\pi S_J^2}} \exp\left(-\frac{(x-\mu_J)^2}{2S_J^2}\right), \tag{11}$$

where μ_J is the average value of M , H J -th phase, S_J - standard deviation of the distribution in *the* J -th phase (StdDev). The theoretical probability density function $_P$ (x) of the distribution of values M , H was determined taking into account the volume fraction *fJ* of each phase

$$P(x) = \sum_{J=1}^{n} f_J p_J(x), \tag{12}$$

where J = 1, 2, 3.

The unknown values μ_J , S_J , f_J were found from the condition of the minimum standard deviation between the experimental discrete values of nanoindentation probability density P_i and the theoretical values $P(x_j)$ in each i -th interval with the additional condition of equality of the sum of the volume fractions of phases f_J unit (m = 100 – number of intervals along the M , H *axis*) [3]:

$$\min \sum_{i=1}^{m} \frac{(P_i - P(x_i))^2}{m}, \tag{13}$$

$$\sum_{J=1}^{n} f_J = 1, \tag{14}$$

where J = 1, 2, 3. To find the minimum of function (13) under additional condition (14) and unknown values μ_J , S_J , f_J, *we used the* MathLab program algorithm.

When conducting research, the following materials were used as the main components:

1) binder-Portland cement PC 500 D0 according to GOST 30515-2013 with the following mineral composition, wt , %: C_3S – 58,31; From $_2$ S – 18,38; C_3A – 8,01; From $_4$ AF – 10,64 ;

2) modifying substances:

a) gyrothermal nanosilica (SiO_2) with the following characteristics: SiO_2 content in ash – 120 g/dm^3, density ρ = 1075 g/dm^3, total salt content – 1720 mg/dm^3, pH = 9,2, specific surface area – 500 m^2 / g and the average diameter of primary SiO_2 nanoparticles is 5,5 nm according to TU 2111-001-97849280-2014;

b) multiwalled carbon nanotubes (MWCNTs): average diameter of tubes and fibers – 10,300 nm , average length of tubes and fibers – 0,01–20 microns, bulk density – 0,15–0,22 g/cm^3 , ash content – no more than 5 %, specific adsorption surface – from 60 m^2 /g according to TU BY 691460594.002-2016;

3) superplasticizer (SP) in the form of an aqueous solution – polycarboxylate copolymer with a density of 1,1–1,14 g/ml, pH = 6–8, viscosity 230–330 cP, content of non-volatile substances - 39–41 %, water-reducing ability over 40 %;

4) water for mixing and subsequent hardening, meeting the requirements of STB 1114-98 and GOST 23732-2011.

Prototypes. Testing using the nanoindentation method was carried out on cement samples No. 1–4 with dimensions of 10 x 10 x 20 mm with additives, the composition of the components of which is given in Table 1.

Table 1 – Composition of the raw material mixture

Sample composition number/test sample number	**Composition of the additive, % by weight of cement**		
	Mass fraction of joint venture	**Mass fraction of solid MWCNT particles**	**SiO_2 solid particles**
1	0,4	–	–
2	0,4	–	0,000 006
3	0,4	0,000 04	–
4	0,4	0,000 04	0,000 006

The additive for samples of compositions No. 1–4 was introduced in an amount of 0,8 % by weight of cement. The amount of mixing water for all samples was selected in such a way that in all cases a dough of normal thickness was obtained. The water-cement ratio of samples of compositions No. 1–4 was W/C = 0,21. Hydrated samples were stored in water at room temperature until testing. Age at nanoindentation and construction of histograms in Figure 4 – 4 months. At this age, the structure of the phases has formed and the duration of point-by-point nanoindentation itself will not affect the results.

Designations

f_c – compressive strength of concrete, MPa; $f_{with\ t}$ – concrete bending strength, MPa; *E* – Young's modulus, GPa; G – shear modulus, GPa; *H* – hardness, GPa; *M* – modulus of elasticity, GPa; *ρ* – density, kg/ m^3. Indices: c – compression; with t – bending.

References

1. Sanchez, F. Nanotechnologies in the production of concrete. Review / F. Sanchez, K. Sobolev // Bulletin of Tomsk State Architecture and Construction university. – 2013. – No. 3 (40). – P. 262–289.

2. Ulm, F. Engineering of Concrete // F. Ulm, J. Nano / Arabian Journal for Science and Engineering. – 2012. – Vol. 37, no. 2. – P. 481–488.

3. Constantinides G. The nanogranular nature of C–S–H / G. Constantinides, F. Ulm // J. Mechanics Phys. Solids. – 2007. – Vol. 55, Issue 1. – P. 64–90.

4. Investigation by atomic force microscopy of forces at the origin of cement cohesion / S. Lesko [et al.] // Ultramicroscopy. – 2001. – Vol. 86, Issue 1–2. – P. 11–21.

5. Study of C–S–H growth on C_3S surface during its early hydration / S. Garrault [et al.] // Materials and Structures. – 2005. – Vol. 38, Issue 4. – P. 435–442.

6. Plassard, C. Investigation of the surface structure and elastic properties of calcium silicate hydrates at the nanoscale / C. Plassard // Ultramicroscopy. – 2004. – Vol. 100, Issue 3–4. – P. 331–338.

7. Preparation of a complex additive for increasing the strength of concrete based on nanodispersed silicon dioxide of hydrothermal solutions / V. V. Potapov [et al.] // Fundamental research. – 2012. – No. 9–2. – P. 404–409.

8. Quantification and characterization of C–S–H in silica nanoparticles incorporated cementitious system / L. P. Singh [et al.] // Cement & Concrete Composites. – 2017. – Vol. 79. – P. 106–116.

9. Modification of Cement Concrete by Admixtures Containing Nanosized Materials / S. A. Zhdanok [et al.] // Journal of Engineering Physics and Thermophysics. – 2020. – Vol. 93, no. 3. – P. 669–673.

11. Intrinsic Elastic Properties of Calcium Silicate Hydrates by Nanoindentation / S. Plassard [et al.] // 12th International Congress on the Chemistry of Cement. – Montreal. Canada, Jul 2007. – P. 44.

12. Microscopic physical basis of the poromechanical behavior of cement-based materials / A. Gmira [et al.] // Materials and Structures. – 2004. – Vol. 37, no. 265. – P. 3–14.

13. Nanoindentation method for studying the structure of modified cement stone / E. N. Polonina [et al.] // Journal of Engineering Physics and Thermophysics. – 2021. – Vol. 94, no. 5. – P. 1194–1207.

14. Mechanism for Improving the Strength of a Cement Material Modified by SiO_2 Nanoparticles and Multiwall Carbon Nanotubes / E. N. Polonina [et al.] // Journal of Engineering Physics and Thermophysics. – 2021. – Vol. 94, no. 1. – P. 67–78.

15. Studying the Structure of a Cement Composite Modified by Hydrothermal SiO2 Nanoparticles and MCNTs by the IR-Spectroscopy Method / E. N. Polonina [et al.] // Journal of Engineering Physics and Thermophysics. – 2022. – Vol. 95, no. 6. – P. 1426–1436.

16. Investigation of the Structure of a Cement Composite Modified by Hydrothermal SiO2 Nanoparticles and MCNT Nanoparticles by the X-Ray Phase Analysis Method. / E. N. Polonina [et al.] // Journal of Engineering Physics and Thermophysics. – 2023. – Vol. 96, no. 1. – P. 215–223.